



Search for Transient Gravitational-wave Signals Associated with Magnetar Bursts during Advanced LIGO's Second Observing Run

B. P. Abbott¹, R. Abbott¹, T. D. Abbott², S. Abraham³, F. Acernese^{4,5}, K. Ackley⁶, C. Adams⁷, R. X. Adhikari¹, V. B. Adya^{8,9}, C. Affeldt^{8,9}, M. Agathos¹⁰, K. Agatsuma¹¹, N. Aggarwal¹², O. D. Aguiar¹³, L. Aiello^{14,15}, A. Ain³, P. Ajith¹⁶, G. Allen¹⁷, A. Allocca^{18,19}, M. A. Aloy²⁰, P. A. Altin²¹, A. Amato²², A. Ananyeva¹, S. B. Anderson¹, W. G. Anderson²³, S. V. Angelova²⁴, S. Antier²⁵, S. Appert¹, K. Arai¹, M. C. Araya¹, J. S. Areeda²⁶, M. Arène²⁷, N. Arnaud^{25,28}, S. Ascenzi^{29,30}, G. Ashton⁶, S. M. Aston⁷, P. Astone³¹, F. Aubin³², P. Aufmuth⁹, K. AultO'Neal³³, C. Austin², V. Avendano³⁴, A. Avila-Alvarez²⁶, S. Babak^{27,35}, P. Bacon²⁷, F. Badaracco^{14,15}, M. K. M. Bader³⁶, S. Bae³⁷, P. T. Baker³⁸, F. Baldaccini^{39,40}, G. Ballardín²⁸, S. W. Ballmer⁴¹, S. Banagiri⁴², J. C. Barayoga¹, S. E. Barclay⁴³, B. C. Barish¹, D. Barker⁴⁴, K. Barkett⁴⁵, S. Barnum¹², F. Barone^{4,5}, B. Barr⁴³, L. Barsotti¹², M. Barsuglia²⁷, D. Barta⁴⁶, J. Bartlett⁴⁴, I. Bartos⁴⁷, R. Bassiri⁴⁸, A. Basti^{18,19}, M. Bawaj^{40,49}, J. C. Bayley⁴³, M. Bazzan^{50,51}, B. Bécsy⁵², M. Bejger^{27,53}, I. Belahcene²⁵, A. S. Bell⁴³, D. Beniwal⁵⁴, B. K. Berger⁴⁸, G. Bergmann^{8,9}, S. Bernuzzi^{55,56}, J. J. Bero⁵⁷, C. P. L. Berry⁵⁸, D. Bersanetti⁵⁹, A. Bertolini³⁶, J. Betzwieser⁷, R. Bhandare⁶⁰, J. Bidler²⁶, I. A. Bilenko⁶¹, S. A. Bilgili³⁸, G. Billingsley¹, J. Birch⁷, R. Birney²⁴, O. Birnholtz⁵⁷, S. Biscans^{1,12}, S. Biscoveanu⁶, A. Bisht⁹, M. Bitossi^{19,28}, M. A. Bizouard²⁵, J. K. Blackburn¹, C. D. Blair⁷, D. G. Blair⁶², R. M. Blair⁴⁴, S. Bloemen⁶³, N. Bode^{8,9}, M. Boer⁶⁴, Y. Boetzel⁶⁵, G. Bogaert⁶⁴, F. Bondu⁶⁶, E. Bonilla⁴⁸, R. Bonnand³², P. Booker^{8,9}, B. A. Boom³⁶, C. D. Booth⁶⁷, R. Bork¹, V. Boschi²⁸, S. Bose^{3,68}, K. Bossie⁷, V. Bossilkov⁶², J. Bosveld⁶², Y. Bouffanais²⁷, A. Bozzi²⁸, C. Bradaschia¹⁹, P. R. Brady²³, A. Bramley⁷, M. Branchesi^{14,15}, J. E. Brau⁶⁹, T. Briant⁷⁰, J. H. Briggs⁴³, F. Brighenti^{71,72}, A. Brillet⁶⁴, M. Brinkmann^{8,9}, V. Brisson^{25,177}, P. Brockill²³, A. F. Brooks¹, D. D. Brown⁵⁴, S. Brunett¹, A. Buikema¹², T. Bulik⁷³, H. J. Bulten^{36,74}, A. Buonanno^{35,75}, D. Buskulic³², C. Buy²⁷, R. L. Byer⁴⁸, M. Cabero^{8,9}, L. Cadonati⁷⁶, G. Cagnoli^{22,77}, C. Cahillane¹, J. Calderón Bustillo⁶, T. A. Callister¹, E. Calloni^{5,78}, J. B. Camp⁷⁹, W. A. Campbell⁶, M. Canepa^{59,80}, K. C. Cannon⁸¹, H. Cao⁵⁴, J. Cao⁸², E. Capocasa²⁷, F. Carbognani²⁸, S. Caride⁸³, M. F. Carney⁵⁸, G. Carullo¹⁸, J. Casanueva Diaz¹⁹, C. Casentini^{29,30}, S. Caudill³⁶, M. Cavaglia⁸⁴, F. Cavalier²⁵, R. Cavalieri²⁸, G. Cella¹⁹, P. Cerdá-Durán²⁰, G. Cerretani^{18,19}, E. Cesarini^{30,85}, O. Chaibi⁶⁴, K. Chakravarti³, S. J. Chamberlain⁸⁶, M. Chan⁴³, S. Chao⁸⁷, P. Charlton⁸⁸, E. A. Chase⁵⁸, E. Chassande-Mottin²⁷, D. Chatterjee²³, M. Chaturvedi⁶⁰, B. D. Cheeseboro³⁸, H. Y. Chen⁸⁹, X. Chen⁶², Y. Chen⁴⁵, H.-P. Cheng⁴⁷, C. K. Cheong⁹⁰, H. Y. Chia⁴⁷, A. Chincarini⁵⁹, A. Chiummo²⁸, G. Cho⁹¹, H. S. Cho⁹², M. Cho⁷⁵, N. Christensen^{64,93}, Q. Chu⁶², S. Chua⁷⁰, K. W. Chung⁹⁰, S. Chung⁶², G. Ciani^{50,51}, A. A. Ciobanu⁵⁴, R. Ciolfi^{94,95}, F. Cipriano⁶⁴, A. Cirone^{59,80}, F. Clara⁴⁴, J. A. Clark⁷⁶, P. Clearwater⁹⁶, F. Cleva⁶⁴, C. Cocchieri⁸⁴, E. Coccia^{14,15}, P.-F. Cohadon⁷⁰, D. Cohen²⁵, R. Colgan⁹⁷, M. Coleoni⁹⁸, C. G. Collette⁹⁹, C. Collins¹¹, L. R. Cominsky¹⁰⁰, M. Constances, Jr.¹³, L. Conti⁵¹, S. J. Cooper¹¹, P. Corban⁷, T. R. Corbitt¹, I. Cordero-Carrión¹⁰¹, K. R. Corley⁹⁷, N. Cornish⁵², A. Corsi⁸³, S. Cortese²⁸, C. A. Costa¹³, R. Cotesta³⁵, M. W. Coughlin¹, S. B. Coughlin^{58,67}, J.-P. Coulon⁶⁴, S. T. Countryman⁹⁷, P. Couvares¹, P. B. Covas⁹⁸, E. E. Cowan⁷⁶, D. M. Coward⁶², M. J. Cowart⁷, D. C. Coyne¹, R. Coyne¹⁰², J. D. E. Creighton²³, T. D. Creighton¹⁰³, J. Cripe², M. Croquette⁷⁰, S. G. Crowder¹⁰⁴, T. J. Cullen², A. Cumming⁴³, L. Cunningham⁴³, E. Cuomo²⁸, T. Dal Canton⁷⁹, G. Dálya¹⁰⁵, S. L. Danilishin^{8,9}, S. D'Antonio³⁰, K. Danzmann^{8,9}, A. Dasgupta¹⁰⁶, C. F. Da Silva Costa⁴⁷, L. E. H. Datrier⁴³, V. Dattilo²⁸, I. Dave⁶⁰, M. Davies²⁵, D. Davis⁴¹, E. J. Daw¹⁰⁷, D. DeBra⁴⁸, M. Deenadayalan³, J. Degallaix²², M. De Laurentis^{5,78}, S. Deléglise⁷⁰, W. Del Pozzo^{18,19}, L. M. DeMarchi⁵⁸, N. Demos¹², T. Dent^{8,9,108}, R. De Pietri^{56,109}, J. Derby²⁶, R. De Rosa^{5,78}, C. De Rossi^{22,28}, R. DeSalvo¹¹⁰, O. de Varona^{8,9}, S. Dhurandhar³, M. C. Díaz¹⁰³, T. Dietrich³⁶, L. Di Fiore⁵, M. Di Giovanni^{95,111}, T. Di Girolamo^{5,78}, A. Di Lieto^{18,19}, B. Ding⁹⁹, S. Di Pace^{31,112}, I. Di Palma^{31,112}, F. Di Renzo^{18,19}, A. Dmitriev¹¹, Z. Doctor⁸⁹, F. Donovan¹², K. L. Dooley^{67,84}, S. Doravari^{8,9}, I. Dorrington⁶⁷, T. P. Downes²³, M. Drago^{14,15}, J. C. Driggers⁴⁴, Z. Du⁸², J.-G. Ducoin²⁵, P. Dupej⁴³, S. E. Dwyer⁴⁴, P. J. Easter⁶, T. B. Edo¹⁰⁷, M. C. Edwards⁹³, A. Effler⁷, P. Ehrens¹, J. Eichholz¹, S. S. Eikenberry⁴⁷, M. Eisenmann³², R. A. Eisenstein¹², R. C. Essick⁸⁹, H. Estelles⁹⁸, D. Estevez³², Z. B. Etienne³⁸, T. Etzel¹, M. Evans¹², T. M. Evans⁷, V. Fafone^{14,29,30}, H. Fair⁴¹, S. Fairhurst⁶⁷, X. Fan⁸², S. Farinon⁵⁹, B. Farr⁶⁹, W. M. Farr¹¹, E. J. Fauchon-Jones⁶⁷, M. Favata³⁴, M. Fays¹⁰⁷, M. Fazio¹¹³, C. Fee¹¹⁴, J. Feicht¹, M. M. Fejer⁴⁸, F. Feng²⁷, A. Fernandez-Galiana¹², I. Ferrante^{18,19}, E. C. Ferreira¹³, T. A. Ferreira¹³, F. Ferrini²⁸, F. Fidecaro^{18,19}, I. Fiori²⁸, D. Fiorucci²⁷, M. Fishbach⁸⁹, R. P. Fisher^{41,115}, J. M. Fishner¹², M. Fitz-Axen⁴², R. Flaminio^{32,116}, M. Fletcher⁴³, E. Flynn²⁶, H. Fong¹¹⁷, J. A. Font^{20,118}, P. W. F. Forsyth²¹, J.-D. Fournier⁶⁴, S. Frasca^{31,112}, F. Frasconi¹⁹, Z. Frei¹⁰⁵, A. Freise¹¹, R. Frey⁶⁹, V. Frey²⁵, P. Fritschel¹², V. V. Frolov⁷, P. Fulda⁴⁷, M. Fyffe⁷, H. A. Gabbard⁴³, B. U. Gadre³, S. M. Gaebel¹¹, J. R. Gair¹¹⁹, L. Gammaitoni³⁹, M. R. Ganija⁵⁴, S. G. Gaonkar³, A. Garcia²⁶, C. García-Quirós⁹⁸, F. Garufi^{5,78}, B. Gateley⁴⁴, S. Gaudio³³, G. Gaur¹²⁰, V. Gayathri¹²¹, G. Gemme⁵⁹, E. Genin²⁸, A. Gennai¹⁹, D. George¹⁷, J. George⁶⁰, L. Gergely¹²², V. Germain³², S. Ghonge⁷⁶, Abhirup Ghosh¹⁶, Archisman Ghosh³⁶, S. Ghosh²³, B. Giacomazzo^{95,111}, J. A. Giaime^{2,7}, K. D. Giardino⁷, A. Giazotto^{19,178}, K. Gill³³, G. Giordano^{4,5}, L. Glover¹¹⁰, P. Godwin⁸⁶, E. Goetz⁴⁴, R. Goetz⁴⁷, B. Goncharov⁶, G. González², J. M. Gonzalez Castro^{18,19}, A. Gopakumar¹²³, M. L. Gorodetsky⁶¹, S. E. Gossan¹, M. Gosselin²⁸, R. Gouaty³², A. Grado^{5,124}, C. Graef⁴³, M. Granata²², A. Grant⁴³, S. Gras¹², P. Grassia¹, C. Gray⁴⁴, R. Gray⁴³, G. Greco^{71,72}, A. C. Green^{11,47}, R. Green⁶⁷, E. M. Gretarsson³³, P. Groot⁶³, H. Grote⁶⁷, S. Grunewald³⁵, P. Gruning²⁵, G. M. Guidi^{71,72}, H. K. Gulati¹⁰⁶, Y. Guo³⁶, A. Gupta⁸⁶, M. K. Gupta¹⁰⁶, E. K. Gustafson¹, R. Gustafson¹²⁵, L. Haegel⁹⁸, O. Halim^{14,15}, B. R. Hall⁶⁸, E. D. Hall¹², E. Z. Hamilton⁶⁷, G. Hammond⁴³, M. Haney⁶⁵,

M. M. Hanke^{8,9}, J. Hanks⁴⁴, C. Hanna⁸⁶, O. A. Hannuksela⁹⁰, J. Hanson⁷, T. Hardwick², K. Haris¹⁶, J. Harms^{14,15}, G. M. Harry¹²⁶, I. W. Harry³⁵, C.-J. Haster¹¹⁷, K. Haughian⁴³, F. J. Hayes⁴³, J. Healy⁵⁷, A. Heidmann⁷⁰, M. C. Heintze⁷, H. Heitmann⁶⁴, P. Hello²⁵, G. Hemming²⁸, M. Hendry⁴³, I. S. Heng⁴³, J. Hennig^{8,9}, A. W. Heptonstall¹, Francisco Hernandez Vivanco⁶, M. Heurs^{8,9}, S. Hild⁴³, T. Hinderer^{36,127,128}, D. Hoak²⁸, S. Hochheim^{8,9}, D. Hofman²², A. M. Holgado¹⁷, N. A. Holland²¹, K. Holt⁷, D. E. Holz⁸⁹, P. Hopkins⁶⁷, C. Horst²³, J. Hough⁴³, E. J. Howell⁶², C. G. Hoy⁶⁷, A. Hreibi⁶⁴, E. A. Huerta¹⁷, D. Huet²⁵, B. Hughey³³, M. Hulko¹, S. Husa⁹⁸, S. H. Huttner⁴³, T. Huynh-Dinh⁷, B. Idzkowski⁷³, A. Iess^{29,30}, C. Ingram⁵⁴, R. Inta⁸³, G. Intini^{31,112}, B. Irwin¹¹⁴, H. N. Isa⁴³, J.-M. Isac⁷⁰, M. Isi¹, B. R. Iyer¹⁶, K. Izumi⁴⁴, T. Jacqmin⁷⁰, S. J. Jadhav¹²⁹, K. Jani⁷⁶, N. N. Janthalur¹²⁹, P. Jaranowski¹³⁰, A. C. Jenkins¹³¹, J. Jiang⁴⁷, D. S. Johnson¹⁷, A. W. Jones¹¹, D. I. Jones¹³², R. Jones⁴³, R. J. G. Jonker³⁶, L. Ju⁶², J. Junker^{8,9}, C. V. Kalaghatgi⁶⁷, V. Kalogera⁵⁸, B. Kamai¹, S. Kandhasamy⁸⁴, G. Kang³⁷, J. B. Kanner¹, S. J. Kapadia²³, S. Karki⁶⁹, K. S. Karvinen^{8,9}, R. Kashyap¹⁶, M. Kasprzak¹, S. Katsanevas²⁸, E. Katsavounidis¹², W. Katzman⁷, S. Kaufer⁹, K. Kawabe⁴⁴, N. V. Keerthana³, F. Kéfélian⁶⁴, D. Keitel⁴³, R. Kennedy¹⁰⁷, J. S. Key¹³³, F. Y. Khalili⁶¹, H. Khan²⁶, I. Khan^{14,30}, S. Khan^{8,9}, Z. Khan¹⁰⁶, E. A. Khazanov¹³⁴, M. Khursheed⁶⁰, N. Kijbunchoo²¹, Chunglee Kim¹³⁵, J. C. Kim¹³⁶, K. Kim⁹⁰, W. Kim⁵⁴, W. S. Kim¹³⁷, Y.-M. Kim¹³⁸, C. Kimball⁵⁸, E. J. King⁵⁴, P. J. King⁴⁴, M. Kinley-Hanlon¹²⁶, R. Kirchhoff^{8,9}, J. S. Kissel⁴⁴, L. Kleybolte¹³⁹, J. H. Klika²³, S. Klimentko⁴⁷, T. D. Knowles³⁸, P. Koch^{8,9}, S. M. Koehlenbeck^{8,9}, G. Koekoek^{36,140}, S. Koley³⁶, V. Kondrashov¹, A. Kontos¹², N. Koper^{8,9}, M. Korobko¹³⁹, W. Z. Korth¹, I. Kowalska⁷³, D. B. Kozak¹, V. Kringel^{8,9}, N. Krishnendu¹⁴¹, A. Królak^{142,143}, G. Kuehn^{8,9}, A. Kumar¹²⁹, P. Kumar¹⁴⁴, R. Kumar¹⁰⁶, S. Kumar¹⁶, L. Kuo⁸⁷, A. Kutynia¹⁴², S. Kwang²³, B. D. Lackey³⁵, K. H. Lai⁹⁰, T. L. Lam⁹⁰, M. Landry⁴⁴, B. B. Lane¹², R. N. Lang¹⁴⁵, J. Lange⁵⁷, B. Lantz⁴⁸, R. K. Lanza¹², A. Lartaux-Vollard²⁵, P. D. Lasky⁶, M. Laxen⁷, A. Lazzarini¹, C. Lazzaro⁵¹, P. Leaci^{31,112}, S. Leavey^{8,9}, Y. K. Leconte⁴⁴, C. H. Lee⁹², H. K. Lee¹⁴⁶, H. M. Lee¹⁴⁷, H. W. Lee¹³⁶, J. Lee⁹¹, K. Lee⁴³, J. Lehmann^{8,9}, A. Lenon³⁸, N. Leroy²⁵, N. Letendre³², Y. Levin^{6,97}, J. Li⁸², K. J. L. Li⁹⁰, T. G. F. Li⁹⁰, X. Li⁴⁵, F. Lin⁶, F. Linde³⁶, S. D. Linker¹¹⁰, T. B. Littenberg¹⁴⁸, J. Liu⁶², X. Liu²³, R. K. L. Lo^{1,90}, N. A. Lockerbie²⁴, L. T. London⁶⁷, A. Longo^{149,150}, M. Lorenzini^{14,15}, V. Lorient¹⁵¹, M. Lormand⁷, G. Losurdo¹⁹, J. D. Lough^{8,9}, C. O. Lousto⁵⁷, G. Lovelace²⁶, M. E. Lower¹⁵², H. Lück^{8,9}, D. Lumaca^{29,30}, A. P. Lundgren¹⁵³, R. Lynch¹², Y. Ma⁴⁵, R. Macas⁶⁷, S. Macfoy²⁴, M. MacInnis¹², D. M. Macleod⁶⁷, A. Macquet⁶⁴, F. Magaña-Sandoval⁴¹, L. Magaña Zertuche⁸⁴, R. M. Magee⁸⁶, E. Majorana³¹, I. Maksimovic¹⁵¹, A. Malik⁶⁰, N. Man⁶⁴, V. Mandic⁴², V. Mangano⁴³, G. L. Mansell^{12,44}, M. Manske^{21,23}, M. Mantovani²⁸, F. Marchesoni^{40,49}, F. Marion³², S. Márka⁹⁷, Z. Márka⁹⁷, C. Markakis^{10,17}, A. S. Markosyan⁴⁸, A. Markowitz¹, E. Maros¹, A. Marquina¹⁰¹, S. Marsat³⁵, F. Martelli^{71,72}, I. W. Martin⁴³, R. M. Martin³⁴, D. V. Martynov¹¹, K. Mason¹², E. Massera¹⁰⁷, A. Masserot³², T. J. Massinger¹, M. Masso-Reid⁴³, S. Mastrogiovanni^{31,112}, A. Matas^{35,42}, F. Matchard^{1,12}, L. Matone⁹⁷, N. Mavalvala¹², N. Mazumder⁶⁸, J. J. McCann⁶², R. McCarthy⁴⁴, D. E. McClelland²¹, S. McCormick⁷, L. McCuller¹², S. C. McGuire¹⁵⁴, J. McIver¹, D. J. McManus²¹, T. McRae²¹, S. T. McWilliams³⁸, D. Meacher⁸⁶, G. D. Meadors⁶, M. Mehmet^{8,9}, A. K. Mehta¹⁶, J. Meidam³⁶, A. Melatos⁹⁶, G. Mendell⁴⁴, R. A. Mercer²³, L. Mereni²², E. L. Merilh⁴⁴, M. Merzougui⁶⁴, S. Meshkov¹, C. Messenger⁴³, C. Messick⁸⁶, R. Metzdrorf⁷⁰, P. M. Meyers⁹⁶, H. Miao¹¹, C. Michel²², H. Middleton⁹⁶, E. E. Mikhailov¹⁵⁵, L. Milano^{5,78}, A. L. Miller⁴⁷, A. Miller^{31,112}, M. Millhouse⁵², J. C. Mills⁶⁷, M. C. Milovich-Goff¹¹⁰, O. Minazzoli^{64,156}, Y. Minenkov³⁰, A. Mishkin⁴⁷, C. Mishra¹⁵⁷, T. Mistry¹⁰⁷, S. Mitra³, V. P. Mitrofanov⁶¹, G. Mitselmakher⁴⁷, R. Mittleman¹², G. Mo⁹³, D. Moffa¹¹⁴, K. Mogushi⁸⁴, S. R. P. Mohapatra¹², M. Montani^{71,72}, C. J. Moore¹⁰, D. Moraru⁴⁴, G. Moreno⁴⁴, S. Morisaki⁸¹, B. Mours³², C. M. Mow-Lowry¹¹, Arunava Mukherjee^{8,9}, D. Mukherjee²³, S. Mukherjee¹⁰³, N. Mukund³, A. Mullavey⁷, J. Munch⁵⁴, E. A. Muñiz⁴¹, M. Muratore³³, P. G. Murray⁴³, A. Nagar^{85,158,159}, I. Nardecchia^{29,30}, L. Naticchioni^{31,112}, R. K. Nayak¹⁶⁰, J. Neilson¹¹⁰, G. Nelemans^{36,63}, T. J. N. Nelson⁷, M. Nery^{8,9}, A. Neunert¹²⁵, K. Y. Ng¹², S. Ng⁵⁴, P. Nguyen⁶⁹, D. Nichols^{36,127}, S. Nissanke^{36,127}, F. Nocera²⁸, C. North⁶⁷, L. K. Nuttall¹⁵³, M. Obergaulinger²⁰, J. Oberling⁴⁴, B. D. O'Brien⁴⁷, G. D. O'Dea¹¹⁰, G. H. Ogil¹⁶¹, J. J. Oh¹³⁷, S. H. Oh¹³⁷, F. Ohme^{8,9}, H. Ohta⁸¹, M. A. Okada¹³, M. Oliver⁹⁸, P. Oppermann^{8,9}, Richard J. Oram⁷, B. O'Reilly⁷, R. G. Ormiston⁴², L. F. Ortega⁴⁷, R. O'Shaughnessy⁵⁷, S. Ossokine³⁵, D. J. Ottaway⁵⁴, H. Overmier⁷, B. J. Owen⁸³, A. E. Pace⁸⁶, G. Pagano^{18,19}, M. A. Page⁶², A. Pai¹²¹, S. A. Pai⁶⁰, J. R. Palamos⁶⁹, O. Palashov¹³⁴, C. Palomba³¹, A. Pal-Singh¹³⁹, Huang-Wei Pan⁸⁷, B. Pang⁴⁵, P. T. H. Pang⁹⁰, C. Pankow⁵⁸, F. Pannarale^{31,112}, B. C. Pant⁶⁰, F. Paoletti¹⁹, A. Paoli²⁸, A. Parida³, W. Parker^{7,154}, D. Pascucci⁴³, A. Pasqualetti²⁸, R. Passaquietti^{18,19}, D. Passuello¹⁹, M. Patil¹⁴³, B. Patricelli^{18,19}, B. L. Pearlstone⁴³, C. Pedersen⁶⁷, M. Pedraza¹, R. Pedurand^{22,162}, A. Pele⁷, S. Penn¹⁶³, C. J. Perez⁴⁴, A. Perreca^{95,111}, H. P. Pfeiffer^{35,117}, M. Phelps^{8,9}, K. S. Phukon³, O. J. Piccinni^{31,112}, M. Pichot⁶⁴, F. Piergiovanni^{71,72}, G. Pillant²⁸, L. Pinard²², M. Pirello⁴⁴, M. Pitkin⁴³, R. Poggiani^{18,19}, D. Y. T. Pong⁹⁰, S. Ponrathnam³, P. Popolizio²⁸, E. K. Porter²⁷, J. Powell¹⁵², A. K. Prajapati¹⁰⁶, J. Prasad³, K. Prasai⁴⁸, R. Prasanna¹²⁹, G. Pratten⁹⁸, T. Prestegard²³, S. Privitera³⁵, G. A. Prodi^{95,111}, L. G. Prokhorov⁶¹, O. Puncken^{8,9}, M. Punturo⁴⁰, P. Puppato³¹, M. Pürer³⁵, H. Qi²³, V. Quetschke¹⁰³, P. J. Quinonez³³, E. A. Quintero¹, R. Quitzow-James⁶⁹, F. J. Raab⁴⁴, H. Radkins⁴⁴, N. Radulescu⁶⁴, P. Raffai¹⁰⁵, S. Raja⁶⁰, C. Rajan⁶⁰, B. Rajbhandari⁸³, M. Rakhmanov¹⁰³, K. E. Ramirez¹⁰³, A. Ramos-Buades⁹⁸, Javed Rana³, K. Rao⁵⁸, P. Rapagnani^{31,112}, V. Raymond⁶⁷, M. Razzano^{18,19}, J. Read²⁶, T. Regimbau³², L. Rei⁵⁹, S. Reid²⁴, D. H. Reitze^{1,47}, W. Ren¹⁷, F. Ricci^{31,112}, C. J. Richardson³³, J. W. Richardson¹, P. M. Ricker¹⁷, K. Riles¹²⁵, M. Rizzo⁵⁸, N. A. Robertson^{1,43}, R. Robie⁴³, F. Robinet²⁵, A. Rocchi³⁰, L. Rolland³², J. G. Rollins¹, V. J. Roma⁶⁹, M. Romanelli⁶⁶, R. Romano^{4,5}, C. L. Romel⁴⁴, J. H. Romie⁷, K. Rose¹¹⁴, D. Rosińska^{53,164}, S. G. Rosofsky¹⁷, M. P. Ross¹⁶⁵, S. Rowan⁴³, A. Rüdiger^{8,9,179}, P. Ruggi²⁸, G. Rutins¹⁶⁶, K. Ryan⁴⁴, S. Sachdev¹, T. Sadecki⁴⁴, M. Sakellariadou¹³¹, L. Salconi²⁸, M. Saleem¹⁴¹, A. Samajdar³⁶, L. Sammut⁶, E. J. Sanchez¹, L. E. Sanchez¹, N. Sanchis-Gual²⁰, V. Sandberg⁴⁴, J. R. Sanders⁴¹, K. A. Santiago³⁴, N. Sarin⁶, B. Sassolas²², P. R. Saulson⁴¹, O. Sauter¹²⁵, R. L. Savage⁴⁴, P. Schale⁶⁹, M. Scheel⁴⁵, J. Scheuer⁵⁸

P. Schmidt⁶³, R. Schnabel¹³⁹, R. M. S. Schofield⁶⁹, A. Schönbeck¹³⁹, E. Schreiber^{8,9}, B. W. Schulte^{8,9}, B. F. Schutz⁶⁷, S. G. Schwalbe³³, J. Scott⁴³, S. M. Scott²¹, E. Seidel¹⁷, D. Sellers⁷, A. S. Sengupta¹⁶⁷, N. Sennett³⁵, D. Sentenac²⁸, V. Sequino^{14,29,30}, A. Sergeev¹³⁴, Y. Setyawati^{8,9}, D. A. Shaddock²¹, T. Shaffer⁴⁴, M. S. Shahriar⁵⁸, M. B. Shaner¹¹⁰, L. Shao³⁵, P. Sharma⁶⁰, P. Shawhan⁷⁵, H. Shen¹⁷, R. Shink¹⁶⁸, D. H. Shoemaker¹², D. M. Shoemaker⁷⁶, S. ShyamSundar⁶⁰, K. Siellez⁷⁶, M. Sieniawska⁵³, D. Sigg⁴⁴, A. D. Silva¹³, L. P. Singer⁷⁹, N. Singh⁷³, A. Singhal^{14,31}, A. M. Sintes⁹⁸, S. Sitmukhambetov¹⁰³, V. Skliris⁶⁷, B. J. J. Slagmolen²¹, T. J. Slaven-Blair⁶², J. R. Smith²⁶, R. J. E. Smith⁶, S. Somala¹⁶⁹, E. J. Son¹³⁷, B. Sorazu⁴³, F. Sorrentino⁵⁹, T. Souradeep³, E. Sowell⁸³, A. P. Spencer⁴³, A. K. Srivastava¹⁰⁶, V. Srivastava⁴¹, K. Staats⁵⁸, C. Stachie⁶⁴, M. Standke^{8,9}, D. A. Steer²⁷, M. Steinke^{8,9}, J. Steinlechner^{43,139}, S. Steinlechner¹³⁹, D. Steinmeyer^{8,9}, S. P. Stevenson¹⁵², D. Stocks⁴⁸, R. Stone¹⁰³, D. J. Stops¹¹, K. A. Strain⁴³, G. Stratta^{71,72}, S. E. Strigin⁶¹, A. Strunk⁴⁴, R. Sturani¹⁷⁰, A. L. Stuver¹⁷¹, V. Sudhir¹², T. Z. Summerscales¹⁷², L. Sun¹, S. Sunil¹⁰⁶, J. Suresh³, P. J. Sutton⁶⁷, B. L. Swinkels³⁶, M. J. Szczepańczyk³³, M. Tacca³⁶, S. C. Tait⁴³, C. Talbot⁶, D. Talukder⁶⁹, D. B. Tanner⁴⁷, M. Tápai¹²², A. Taracchini³⁵, J. D. Tasson⁹³, R. Taylor¹, F. Thies^{8,9}, M. Thomas⁷, P. Thomas⁴⁴, S. R. Thondapu⁶⁰, K. A. Thorne⁷, E. Thrane⁶, Shubhanshu Tiwari^{95,111}, Srishti Tiwari¹²³, V. Tiwari⁶⁷, K. Toland⁴³, M. Tonelli^{18,19}, Z. Tornasi⁴³, A. Torres-Forné¹⁷³, C. I. Torrie¹, D. Töyrä¹¹, F. Travasso^{28,40}, G. Traylor⁷, M. C. Tringali⁷³, A. Trovato²⁷, L. Trozzo^{19,174}, R. Trudeau¹, K. W. Tsang³⁶, M. Tse¹², R. Tso⁴⁵, L. Tsukada⁸¹, D. Tsuna⁸¹, D. Tuyenbayev¹⁰³, K. Ueno⁸¹, D. Ugolini¹⁷⁵, C. S. Unnikrishnan¹²³, A. L. Urban², S. A. Usman⁶⁷, H. Vahlbruch⁹, G. Vajente¹, G. Valdes², N. van Bakel³⁶, M. van Beuzekom³⁶, J. F. J. van den Brand^{36,74}, C. Van Den Broeck^{36,176}, D. C. Vander-Hyde⁴¹, J. V. van Heijningen⁶², L. van der Schaaf³⁶, A. A. van Veggel⁴³, M. Vardaro^{50,51}, V. Varma⁴⁵, S. Vass¹, M. Vasúth⁴⁶, A. Vecchio¹¹, G. Vedovato⁵¹, J. Veitch⁴³, P. J. Veitch⁵⁴, K. Venkateswara¹⁶⁵, G. Venugopalan¹, D. Verkindt³², F. Vetrano^{71,72}, A. Vicere^{71,72}, A. D. Viets²³, D. J. Vine¹⁶⁶, J.-Y. Vinet⁶⁴, S. Vitale¹², T. Vo⁴¹, H. Vocca^{39,40}, C. Vorvick⁴⁴, S. P. Vyatchanin⁶¹, A. R. Wade¹, L. E. Wade¹¹⁴, M. Wade¹¹⁴, R. Walet³⁶, M. Walker²⁶, L. Wallace¹, S. Walsh²³, G. Wang^{14,19}, H. Wang¹¹, J. Z. Wang¹²⁵, W. H. Wang¹⁰³, Y. F. Wang⁹⁰, R. L. Ward²¹, Z. A. Warden³³, J. Warner⁴⁴, M. Was³², J. Watchi⁹⁹, B. Weaver⁴⁴, L.-W. Wei^{8,9}, M. Weinert^{8,9}, A. J. Weinstein¹, R. Weiss¹², F. Wellmann^{8,9}, L. Wen⁶², E. K. Wessel¹⁷, P. Weßels^{8,9}, J. W. Westhouse³³, K. Wette²¹, J. T. Whelan⁵⁷, B. F. Whiting⁴⁷, C. Whittle¹², D. M. Wilken^{8,9}, D. Williams⁴³, A. R. Williamson^{36,127}, J. L. Willis¹, B. Willke^{8,9}, M. H. Wimmer^{8,9}, W. Winkler^{8,9}, C. C. Wipf¹, H. Wittel^{8,9}, G. Woan⁴³, J. Woehler^{8,9}, J. K. Wofford⁵⁷, J. Worden⁴⁴, J. L. Wright⁴³, D. S. Wu^{8,9}, D. M. Wysocki⁵⁷, L. Xiao¹, H. Yamamoto¹, C. C. Yancey⁷⁵, L. Yang¹¹³, M. J. Yap²¹, M. Yazback⁴⁷, D. W. Yeeles⁶⁷, Hang Yu¹², Haocun Yu¹², S. H. R. Yuen⁹⁰, M. Yvert³², A. K. Zadrożny^{103,142}, M. Zanolin³³, T. Zelenova²⁸, J.-P. Zendri⁵¹, M. Zevin⁵⁸, J. Zhang⁶², L. Zhang¹, T. Zhang⁴³, C. Zhao⁶², M. Zhou⁵⁸, Z. Zhou⁵⁸, X. J. Zhu⁶, M. E. Zucker^{1,12}, and J. Zweizig¹

¹ LIGO, California Institute of Technology, Pasadena, CA 91125, USA

² Louisiana State University, Baton Rouge, LA 70803, USA

³ Inter-University Centre for Astronomy and Astrophysics, Pune 411007, India

⁴ Università di Salerno, Fisciano, I-84084 Salerno, Italy

⁵ INFN, Sezione di Napoli, Complesso Universitario di Monte S. Angelo, I-80126 Napoli, Italy

⁶ OzGrav, School of Physics & Astronomy, Monash University, Clayton 3800, Victoria, Australia

⁷ LIGO Livingston Observatory, Livingston, LA 70754, USA

⁸ Max Planck Institute for Gravitational Physics (Albert Einstein Institute), D-30167 Hannover, Germany

⁹ Leibniz Universität Hannover, D-30167 Hannover, Germany

¹⁰ University of Cambridge, Cambridge CB2 1TN, UK

¹¹ University of Birmingham, Birmingham B15 2TT, UK

¹² LIGO, Massachusetts Institute of Technology, Cambridge, MA 02139, USA

¹³ Instituto Nacional de Pesquisas Espaciais, 12227-010 São José dos Campos, São Paulo, Brazil

¹⁴ Gran Sasso Science Institute (GSSI), I-67100 L'Aquila, Italy

¹⁵ INFN, Laboratori Nazionali del Gran Sasso, I-67100 Assergi, Italy

¹⁶ International Centre for Theoretical Sciences, Tata Institute of Fundamental Research, Bengaluru 560089, India

¹⁷ NCSA, University of Illinois at Urbana-Champaign, Urbana, IL 61801, USA

¹⁸ Università di Pisa, I-56127 Pisa, Italy

¹⁹ INFN, Sezione di Pisa, I-56127 Pisa, Italy

²⁰ Departamento de Astronomía y Astrofísica, Universitat de València, E-46100 Burjassot, València, Spain

²¹ OzGrav, Australian National University, Canberra, Australian Capital Territory 0200, Australia

²² Laboratoire des Matériaux Avancés (LMA), CNRS/IN2P3, F-69622 Villeurbanne, France

²³ University of Wisconsin-Milwaukee, Milwaukee, WI 53201, USA

²⁴ SUPA, University of Strathclyde, Glasgow G1 1XQ, UK

²⁵ LAL, Univ. Paris-Sud, CNRS/IN2P3, Université Paris-Saclay, F-91898 Orsay, France

²⁶ California State University Fullerton, Fullerton, CA 92831, USA

²⁷ APC, AstroParticule et Cosmologie, Université Paris Diderot, CNRS/IN2P3, CEA/Irfu, Observatoire de Paris, Sorbonne Paris Cité, F-75205 Paris Cedex 13, France

²⁸ European Gravitational Observatory (EGO), I-56021 Cascina, Pisa, Italy

²⁹ Università di Roma Tor Vergata, I-00133 Roma, Italy

³⁰ INFN, Sezione di Roma Tor Vergata, I-00133 Roma, Italy

³¹ INFN, Sezione di Roma, I-00185 Roma, Italy

³² Laboratoire d'Annecy de Physique des Particules (LAPP), Univ. Grenoble Alpes, Université Savoie Mont Blanc, CNRS/IN2P3, F-74941 Annecy, France

³³ Embry-Riddle Aeronautical University, Prescott, AZ 86301, USA

³⁴ Montclair State University, Montclair, NJ 07043, USA

³⁵ Max Planck Institute for Gravitational Physics (Albert Einstein Institute), D-14476 Potsdam-Golm, Germany

³⁶ Nikhef, Science Park 105, 1098 XG Amsterdam, The Netherlands

³⁷ Korea Institute of Science and Technology Information, Daejeon 34141, Republic of Korea

³⁸ West Virginia University, Morgantown, WV 26506, USA

- ³⁹ Università di Perugia, I-06123 Perugia, Italy
⁴⁰ INFN, Sezione di Perugia, I-06123 Perugia, Italy
⁴¹ Syracuse University, Syracuse, NY 13244, USA
⁴² University of Minnesota, Minneapolis, MN 55455, USA
⁴³ SUPA, University of Glasgow, Glasgow G12 8QQ, UK
⁴⁴ LIGO Hanford Observatory, Richland, WA 99352, USA
⁴⁵ Caltech CaRT, Pasadena, CA 91125, USA
⁴⁶ Wigner RCP, RMKI, H-1121 Budapest, Konkoly Thege Miklós út 29-33, Hungary
⁴⁷ University of Florida, Gainesville, FL 32611, USA
⁴⁸ Stanford University, Stanford, CA 94305, USA
⁴⁹ Università di Camerino, Dipartimento di Fisica, I-62032 Camerino, Italy
⁵⁰ Università di Padova, Dipartimento di Fisica e Astronomia, I-35131 Padova, Italy
⁵¹ INFN, Sezione di Padova, I-35131 Padova, Italy
⁵² Montana State University, Bozeman, MT 59717, USA
⁵³ Nicolaus Copernicus Astronomical Center, Polish Academy of Sciences, 00-716, Warsaw, Poland
⁵⁴ OzGrav, University of Adelaide, Adelaide, South Australia 5005, Australia
⁵⁵ Theoretisch-Physikalisches Institut, Friedrich-Schiller-Universität Jena, D-07743 Jena, Germany
⁵⁶ INFN, Sezione di Milano Bicocca, Gruppo Collegato di Parma, I-43124 Parma, Italy
⁵⁷ Rochester Institute of Technology, Rochester, NY 14623, USA
⁵⁸ Center for Interdisciplinary Exploration & Research in Astrophysics (CIERA), Northwestern University, Evanston, IL 60208, USA
⁵⁹ INFN, Sezione di Genova, I-16146 Genova, Italy
⁶⁰ RRCAT, Indore, Madhya Pradesh 452013, India
⁶¹ Faculty of Physics, Lomonosov Moscow State University, Moscow 119991, Russia
⁶² OzGrav, University of Western Australia, Crawley, Western Australia 6009, Australia
⁶³ Department of Astrophysics/IMAPP, Radboud University Nijmegen, P.O. Box 9010, 6500 GL Nijmegen, The Netherlands
⁶⁴ Artemis, Université Côte d’Azur, Observatoire Côte d’Azur, CNRS, CS 34229, F-06304 Nice Cedex 4, France
⁶⁵ Physik-Institut, University of Zurich, Winterthurerstrasse 190, 8057 Zurich, Switzerland
⁶⁶ Univ Rennes, CNRS, Institut FOTON—UMR6082, F-3500 Rennes, France
⁶⁷ Cardiff University, Cardiff CF24 3AA, UK
⁶⁸ Washington State University, Pullman, WA 99164, USA
⁶⁹ University of Oregon, Eugene, OR 97403, USA
⁷⁰ Laboratoire Kastler Brossel, Sorbonne Université, CNRS, ENS-Université PSL, Collège de France, F-75005 Paris, France
⁷¹ Università degli Studi di Urbino “Carlo Bo,” I-61029 Urbino, Italy
⁷² INFN, Sezione di Firenze, I-50019 Sesto Fiorentino, Firenze, Italy
⁷³ Astronomical Observatory Warsaw University, 00-478 Warsaw, Poland
⁷⁴ VU University Amsterdam, 1081 HV Amsterdam, The Netherlands
⁷⁵ University of Maryland, College Park, MD 20742, USA
⁷⁶ School of Physics, Georgia Institute of Technology, Atlanta, GA 30332, USA
⁷⁷ Université Claude Bernard Lyon 1, F-69622 Villeurbanne, France
⁷⁸ Università di Napoli “Federico II,” Complesso Universitario di Monte S. Angelo, I-80126 Napoli, Italy
⁷⁹ NASA Goddard Space Flight Center, Greenbelt, MD 20771, USA
⁸⁰ Dipartimento di Fisica, Università degli Studi di Genova, I-16146 Genova, Italy
⁸¹ RESCEU, University of Tokyo, Tokyo, 113-0033, Japan
⁸² Tsinghua University, Beijing 100084, People’s Republic of China
⁸³ Texas Tech University, Lubbock, TX 79409, USA
⁸⁴ The University of Mississippi, University, MS 38677, USA
⁸⁵ Museo Storico della Fisica e Centro Studi e Ricerche “Enrico Fermi”, I-00184 Roma, Italy
⁸⁶ The Pennsylvania State University, University Park, PA 16802, USA
⁸⁷ National Tsing Hua University, Hsinchu City, 30013 Taiwan, Republic of China
⁸⁸ Charles Sturt University, Wagga Wagga, New South Wales 2678, Australia
⁸⁹ University of Chicago, Chicago, IL 60637, USA
⁹⁰ The Chinese University of Hong Kong, Shatin, NT, Hong Kong
⁹¹ Seoul National University, Seoul 08826, Republic of Korea
⁹² Pusan National University, Busan 46241, Republic of Korea
⁹³ Carleton College, Northfield, MN 55057, USA
⁹⁴ INAF, Osservatorio Astronomico di Padova, I-35122 Padova, Italy
⁹⁵ INFN, Trento Institute for Fundamental Physics and Applications, I-38123 Povo, Trento, Italy
⁹⁶ OzGrav, University of Melbourne, Parkville, Victoria 3010, Australia
⁹⁷ Columbia University, New York, NY 10027, USA
⁹⁸ Universitat de les Illes Balears, IAC3—IEEC, E-07122 Palma de Mallorca, Spain
⁹⁹ Université Libre de Bruxelles, Brussels B-1050, Belgium
¹⁰⁰ Sonoma State University, Rohnert Park, CA 94928, USA
¹⁰¹ Departamento de Matemáticas, Universitat de València, E-46100 Burjassot, València, Spain
¹⁰² University of Rhode Island, Kingston, RI 02881, USA
¹⁰³ The University of Texas Rio Grande Valley, Brownsville, TX 78520, USA
¹⁰⁴ Bellevue College, Bellevue, WA 98007, USA
¹⁰⁵ MTA-ELTE Astrophysics Research Group, Institute of Physics, Eötvös University, Budapest 1117, Hungary
¹⁰⁶ Institute for Plasma Research, Bhat, Gandhinagar 382428, India
¹⁰⁷ The University of Sheffield, Sheffield S10 2TN, UK
¹⁰⁸ IGFAE, Campus Sur, Universidade de Santiago de Compostela, E-15782 Spain
¹⁰⁹ Dipartimento di Scienze Matematiche, Fisiche e Informatiche, Università di Parma, I-43124 Parma, Italy
¹¹⁰ California State University, Los Angeles, 5151 State University Drive, Los Angeles, CA 90032, USA
¹¹¹ Università di Trento, Dipartimento di Fisica, I-38123 Povo, Trento, Italy
¹¹² Università di Roma “La Sapienza,” I-00185 Roma, Italy
¹¹³ Colorado State University, Fort Collins, CO 80523, USA
¹¹⁴ Kenyon College, Gambier, OH 43022, USA

- ¹¹⁵ Christopher Newport University, Newport News, VA 23606, USA
- ¹¹⁶ National Astronomical Observatory of Japan, 2-21-1 Osawa, Mitaka, Tokyo 181-8588, Japan
- ¹¹⁷ Canadian Institute for Theoretical Astrophysics, University of Toronto, Toronto, Ontario M5S 3H8, Canada
- ¹¹⁸ Observatori Astronòmic, Universitat de València, E-46980 Paterna, València, Spain
- ¹¹⁹ School of Mathematics, University of Edinburgh, Edinburgh EH9 3FD, UK
- ¹²⁰ Institute of Advanced Research, Gandhinagar 382426, India
- ¹²¹ Indian Institute of Technology Bombay, Powai, Mumbai 400 076, India
- ¹²² University of Szeged, Dóm tér 9, Szeged 6720, Hungary
- ¹²³ Tata Institute of Fundamental Research, Mumbai 400005, India
- ¹²⁴ INAF, Osservatorio Astronomico di Capodimonte, I-80131, Napoli, Italy
- ¹²⁵ University of Michigan, Ann Arbor, MI 48109, USA
- ¹²⁶ American University, Washington, DC 20016, USA
- ¹²⁷ GRAPPA, Anton Pannekoek Institute for Astronomy and Institute of High-Energy Physics, University of Amsterdam, Science Park 904, 1098 XH Amsterdam, The Netherlands
- ¹²⁸ Delta Institute for Theoretical Physics, Science Park 904, 1090 GL Amsterdam, The Netherlands
- ¹²⁹ Directorate of Construction, Services & Estate Management, Mumbai 400094, India
- ¹³⁰ University of Białystok, 15-424 Białystok, Poland
- ¹³¹ King's College London, University of London, London WC2R 2LS, UK
- ¹³² University of Southampton, Southampton SO17 1BJ, UK
- ¹³³ University of Washington Bothell, Bothell, WA 98011, USA
- ¹³⁴ Institute of Applied Physics, Nizhny Novgorod, 603950, Russia
- ¹³⁵ Ewha Womans University, Seoul 03760, Republic of Korea
- ¹³⁶ Inje University Gimhae, South Gyeongsang 50834, Republic of Korea
- ¹³⁷ National Institute for Mathematical Sciences, Daejeon 34047, Republic of Korea
- ¹³⁸ Ulsan National Institute of Science and Technology, Ulsan 44919, Republic of Korea
- ¹³⁹ Universität Hamburg, D-22761 Hamburg, Germany
- ¹⁴⁰ Maastricht University, P.O. Box 616, 6200 MD Maastricht, The Netherlands
- ¹⁴¹ Chennai Mathematical Institute, Chennai 603103, India
- ¹⁴² NCBJ, 05-400 Świerk-Otwock, Poland
- ¹⁴³ Institute of Mathematics, Polish Academy of Sciences, 00656 Warsaw, Poland
- ¹⁴⁴ Cornell University, Ithaca, NY 14850, USA
- ¹⁴⁵ Hillsdale College, Hillsdale, MI 49242, USA
- ¹⁴⁶ Hanyang University, Seoul 04763, Republic of Korea
- ¹⁴⁷ Korea Astronomy and Space Science Institute, Daejeon 34055, Republic of Korea
- ¹⁴⁸ NASA Marshall Space Flight Center, Huntsville, AL 35811, USA
- ¹⁴⁹ Dipartimento di Matematica e Fisica, Università degli Studi Roma Tre, I-00146 Roma, Italy
- ¹⁵⁰ INFN, Sezione di Roma Tre, I-00146 Roma, Italy
- ¹⁵¹ ESPCI, CNRS, F-75005 Paris, France
- ¹⁵² OzGrav, Swinburne University of Technology, Hawthorn VIC 3122, Australia
- ¹⁵³ University of Portsmouth, Portsmouth, PO1 3FX, UK
- ¹⁵⁴ Southern University and A&M College, Baton Rouge, LA 70813, USA
- ¹⁵⁵ College of William and Mary, Williamsburg, VA 23187, USA
- ¹⁵⁶ Centre Scientifique de Monaco, 8 quai Antoine 1er, MC-98000, Monaco
- ¹⁵⁷ Indian Institute of Technology Madras, Chennai 600036, India
- ¹⁵⁸ INFN Sezione di Torino, Via P. Giuria 1, I-10125 Torino, Italy
- ¹⁵⁹ Institut des Hautes Etudes Scientifiques, F-91440 Bures-sur-Yvette, France
- ¹⁶⁰ IISER-Kolkata, Mohanpur, West Bengal 741252, India
- ¹⁶¹ Whitman College, 345 Boyer Avenue, Walla Walla, WA 99362 USA
- ¹⁶² Université de Lyon, F-69361 Lyon, France
- ¹⁶³ Hobart and William Smith Colleges, Geneva, NY 14456, USA
- ¹⁶⁴ Janusz Gil Institute of Astronomy, University of Zielona Góra, 65-265 Zielona Góra, Poland
- ¹⁶⁵ University of Washington, Seattle, WA 98195, USA
- ¹⁶⁶ SUPA, University of the West of Scotland, Paisley PA1 2BE, UK
- ¹⁶⁷ Indian Institute of Technology, Gandhinagar Ahmedabad Gujarat 382424, India
- ¹⁶⁸ Université de Montréal/Polytechnique, Montreal, Quebec H3T 1J4, Canada
- ¹⁶⁹ Indian Institute of Technology Hyderabad, Sangareddy, Khandi, Telangana 502285, India
- ¹⁷⁰ International Institute of Physics, Universidade Federal do Rio Grande do Norte, Natal RN 59078-970, Brazil
- ¹⁷¹ Villanova University, 800 Lancaster Ave, Villanova, PA 19085, USA
- ¹⁷² Andrews University, Berrien Springs, MI 49104, USA
- ¹⁷³ Max Planck Institute for Gravitationalphysik (Albert Einstein Institute), D-14476 Potsdam-Golm, Germany
- ¹⁷⁴ Università di Siena, I-53100 Siena, Italy
- ¹⁷⁵ Trinity University, San Antonio, TX 78212, USA
- ¹⁷⁶ Van Swinderen Institute for Particle Physics and Gravity, University of Groningen, Nijenborgh 4, 9747 AG Groningen, The Netherlands

Received 2019 February 9; revised 2019 March 6; accepted 2019 March 6; published 2019 April 4

Abstract

We present the results of a search for short- and intermediate-duration gravitational-wave signals from four magnetar bursts in Advanced LIGO's second observing run. We find no evidence of a signal and set upper bounds on the root sum squared of the total dimensionless strain (h_{rss}) from incoming intermediate-duration gravitational waves ranging from 1.1×10^{-22} at 150 Hz to 4.4×10^{-22} at 1550 Hz at 50% detection efficiency. From the

¹⁷⁷ Deceased, 2018 February.

¹⁷⁸ Deceased, 2017 November.

¹⁷⁹ Deceased, 2018 July.

known distance to the magnetar SGR 1806–20 (8.7 kpc), we can place upper bounds on the isotropic gravitational-wave energy of 3.4×10^{44} erg at 150 Hz assuming optimal orientation. This represents an improvement of about a factor of 10 in strain sensitivity from the previous search for such signals, conducted during initial LIGO’s sixth science run. The short-duration search yielded upper limits of 2.1×10^{44} erg for short white noise bursts, and 2.3×10^{47} erg for 100 ms long ringdowns at 1500 Hz, both at 50% detection efficiency.

Key words: gravitational waves – stars: magnetars

Supporting material: data behind figures

1. Introduction

So far, the Laser Interferometer Gravitational-Wave Observatory (LIGO; Aasi et al. 2015) and Virgo (Acernese et al. 2015) have reported detections of a handful of gravitational-wave (GW) signals from the coalescence of compact binary systems (Abbott et al. 2016a, 2016b, 2017b, 2017c, 2017d, 2017e). Isolated compact objects may also emit detectable GWs, though they are predicted to be much weaker than compact binary coalescences (Sathyaprakash & Schutz 2009). Because of the high energies and mass densities required to generate detectable GWs, neutron stars and supernovae are among the main targets of nonbinary searches. This paper focuses on a type of neutron star: magnetars.

Magnetars are highly magnetized isolated neutron stars (Woods & Thompson 2006; Mereghetti et al. 2015). Originally classified as anomalous X-ray pulsars (AXPs), or soft gamma repeaters (SGRs), some AXPs have been observed acting like SGRs and vice versa. They are now considered to be a single class of objects defined by their power source: the star’s magnetic field, which, at 10^{13} – 10^{15} G, is about $100\times$ stronger than a typical neutron star. Magnetars occasionally emit short bursts of soft γ -rays, but the exact mechanism responsible for the bursts is unclear. There are currently 23 known magnetars (and an additional six candidates; Olausen & Kaspi 2014),¹⁸⁰ which were identified based on observations across wavelengths of bursts, continuous pulsating emission, spindown rates, and glitches in their rotational frequency. The bursts last ~ 0.1 s with luminosity of up to $\sim 2 \times 10^{42}$ erg s⁻¹, and can usually be localized well enough to allow identification of the source magnetar. Many magnetars also emit pulsed X-rays and some are visible in radio.

The large energies involved originally led to the belief that magnetar bursts could be promising sources of detectable GWs, e.g., Ioka (2001) and Corsi & Owen (2011). Further theoretical investigation indicates that most mechanisms are likely too weak to be detectable by current detectors (Levin & van Hoven 2011; Zink et al. 2012). Nevertheless, due to the large amount of energy stored in their magnetic fields and known transient activity, magnetars remain a promising source of GW detections for ground-based detectors with rich underlying physics.

The search presented in this paper is triggered following the identification of magnetar bursts by γ -ray telescopes. The methodology is similar to the one done during initial LIGO’s sixth science run (Quitow-James 2016; Quitow-James et al. 2017), with a few improvements and the use of an additional pipeline targeted toward shorter duration signals (X-Pipeline; Sutton et al. 2010). This pipeline has been used to look for GWs coincident with γ -ray bursts (GRBs; see

Abbott et al. 2017a for such searches during advanced LIGO’s first observing run).

The first searches for GW counterparts from magnetar activity targeted the 2004 hyperflare of SGR 1806–20. Initial LIGO data were used to constrain the GW emission associated with the quasiperiodic seismic oscillations (QPOs) of the magnetar following this catastrophic cosmic event (Abbott et al. 2007; Matone & Márka 2007) as well as the instantaneous gravitational emission (Kalmus et al. 2007; Abbott et al. 2008). Abbott et al. (2008) and Abadie et al. (2011) reported on GW emission limits associated with additional magnetar activity observed during the initial detector era until 2009 June. LIGO data coinciding with the 2006 SGR 1900+14 storm was additionally analyzed by “stacking” GW data (Kalmus et al. 2009) corresponding to individual bursts in the storm’s EM light curve (Abbott et al. 2009). Additionally, a magnetar was considered as a possible source for a GRB during initial LIGO (GRB 051103), and a search using X-Pipeline and the Flare pipeline placed upper limits on GW emission from the star’s fundamental ringing mode (Abadie et al. 2012).

The rest of this paper is laid out as follows: in Section 2, we provide a brief overview of the astrophysics of magnetars as is relevant to GW astronomy and the short bursts used in this analysis. Next, in Section 3, we describe the methodology of the GW search. Section 4 describes the results and upper limits on possible gravitational radiation from the studied bursts. Appendix B contains a discussion of the effect of GW polarization on the sensitivity of the intermediate-duration search.

2. Magnetar Bursts

Magnetars are currently not well understood. Their magnetic fields are strong and complex (Braithwaite & Spruit 2006), and power the star’s activity. Occasionally and unpredictably, magnetars give off short bursts of γ -rays whose exact mechanism is unknown, but may be caused by seismic events, Alfvén waves in the star’s atmosphere, magnetic reconnection events, or some combination of these; see, e.g., Thompson & Duncan (1995). After some of the brighter bursts (giant flares, which have been seen only three times), there is a soft X-ray tail that lasts for hundreds of seconds. QPOs have been observed in the tail of giant flares (Israel et al. 2005; Strohmayer & Watts 2005) and some short bursts (Huppenkothen et al. 2014a, 2014b), during which various frequencies appear, stay for hundreds of seconds, and then disappear again, indicating a resonance within the magnetar. Many possible resonant modes in the core and crust of the magnetar have been suggested to cause the QPOs, although it is unclear which modes actually produce them. Some of these modes, such as f-modes and r-modes, couple well to GWs, and so, if sufficiently excited, could produce detectable GWs, though current models indicate that they will be too weak (Levin & van Hoven 2011; Zink et al. 2012). Other modes, such

¹⁸⁰ See the catalog at <http://www.physics.mcgill.ca/~pulsar/magnetar/main.html>.

Table 1
List of Magnetar Bursts Considered in This GW Search

Source	Date	Time (UTC)	Duration (s)	Fluence (erg cm^{-2})	Distance (kpc)
SGR 1806–20	2017 Feb 11	21:51:58	0.256	8.9×10^{-11}	8.7
SGR 1806–20	2017 Feb 25	06:15:07	0.016	1.2×10^{-11}	8.7
GRB 170304A	2017 Mar 4	00:04:26	0.16	3.1×10^{-10}	...
SGR 1806–20	2017 Apr 29	17:00:44	0.008	1.4×10^{-11}	8.7

Note. GRB 170304A is described in GCN Circular 20813; data on the SGR 1806–20 burst activity are courtesy of David M. Palmer.

as the lowest order torsional mode, do not create the time-changing quadrupole moment needed for GW emission. None of these models provide precise predictions for emitted GW waveforms.

This search was performed on data coincident with the four short bursts from magnetars during advanced LIGO’s second observing run for which there was sufficient data (we require data from two detectors) for both short- (less than a second long) and intermediate-duration (hundreds of seconds long) signals. Table 1 describes the four bursts. In addition to the four studied bursts, there were five bursts that occurred during times when at least one detector was offline. No GW analysis was done on them. All GW detector data come from the two LIGO detectors because Virgo was not taking data during any of these bursts.

Three bursts come from the magnetar SGR 1806–20. They were all identified by the Burst Alert Telescope (BAT) aboard NASA’s *Swift* satellite (Gehrels et al. 2004). These were subthreshold events that were found in BAT data (D. M. Palmer 2017, personal communication), an example of which is shown in Figure 1, with the data from the other two found in Appendix C. The fourth was a short GRB with a soft spectrum observed by the *Fermi* Gamma-ray Burst Monitor (Atwood et al. 2009) and named GRB 170304A.

3. Method

3.1. Excess Power Searches

Fundamentally, all multidetector GW searches seek to identify GW signals that are consistent with the data collected at both detectors. Some searches identify candidate signals in each detector separately, then later consider only the candidates that occur in all detectors within the light-travel time and with the same signal parameters. This approach is disfavored in searches that do not rely on templates. We cannot perform a templated search here because there is no current model that can produce templates for magnetar GW bursts. Instead, we first combine the two data streams to create a time–frequency map where the value in each time–frequency pixel represents some measure of the GWs (often energy) consistent with the observations from the detectors.

The next step is to identify GW signals in the time–frequency map. This is done by clustering together groups of pixels, calculating the significance of each cluster with a metric, and searching for the most significant cluster. In order to cover a broader range of frequencies and timescales, we use two different analysis pipelines, which use different clustering algorithms.

The short-duration search uses seed-based clustering implemented by X-Pipeline, which focuses on groups of bright pixels (the seed; Sutton et al. 2010). Specifically, the clusters

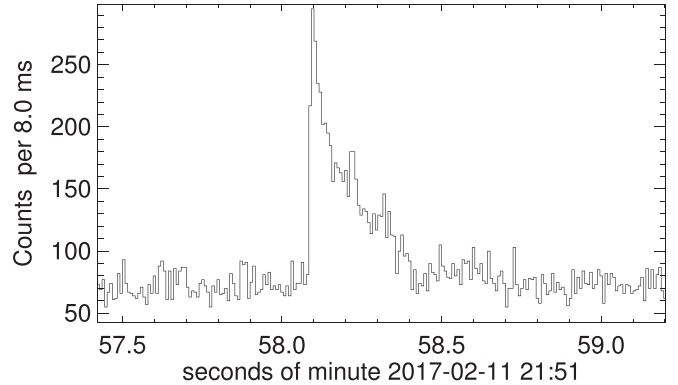


Figure 1. *Swift* BAT’s data for the February 11 burst from SGR 1806–20. Image courtesy of David M. Palmer.

considered by X-Pipeline are groups of neighboring pixels that are all louder than a chosen threshold. This approach works well for short-duration searches, but fails for longer duration signals for two reasons: random noise will tend to break up the signal into multiple clusters, and each pixel is closer to the background, so fewer of them will be above the threshold.

We rely on STAMP (Thrane et al. 2011) for the intermediate-duration search. STAMP offers a seedless method whose clustering algorithm integrates over many, randomly chosen Bézier curves (Thrane & Coughlin 2013, 2014). Because of this, it can jump over gaps in clusters caused by noise, and thus it is better suited for longer duration signals. Additionally, it can build up the signal-to-noise ratio (S/N) over many pixels of only slightly elevated S/N. This method was previously used to search for signals from magnetars during initial LIGO (Quitow-James 2016; Quitow-James et al. 2017).

3.2. X-Pipeline

X-Pipeline is a software package designed to search for short-duration GW signals in multiple detectors and includes automatic glitch rejection, background calculation, and software injection processing (for details, see Sutton et al. 2010). It forms coherent combinations from multiple detectors, thus making it relatively insensitive to non-GW signals, such as instrumental artifacts. X-Pipeline is used primarily to search for GWs coincident with GRBs, but is suitable for any short-duration coherent search.

X-Pipeline takes a likelihood approach to estimating the GW energy found in each time–frequency pixel. It models the data collected at the detectors as a combination of signal and detector noise, then uses a maximum-likelihood technique to calculate the estimated GW signal power in each time–frequency pixel.

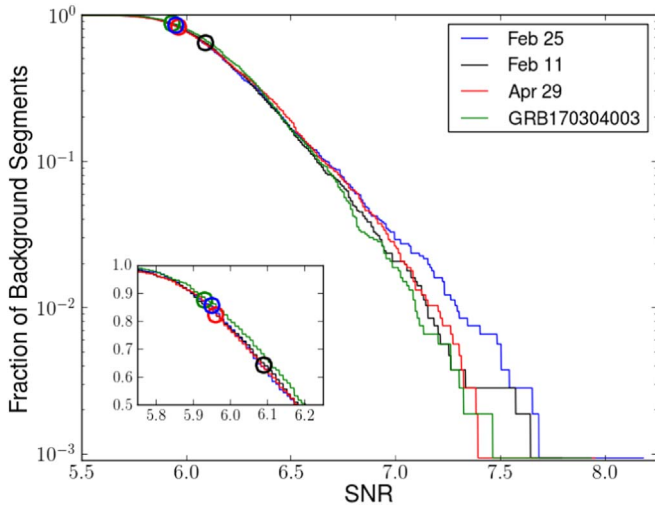


Figure 2. S/N distribution of the background (lines) and on-source result (open circles) for each burst for the intermediate-duration search. As expected, the background distributions are similar; because many background analyses give higher S/N than the on-source results, we conclude that no signal has been detected. Inset: a detailed view of the on-source results. The data used to create this figure are available.

For clustering, X-Pipeline selects the loudest 1% of pixels and connects neighboring pixels. Each connected group is a cluster, and the clusters are scored based on the likelihood described in the previous paragraph. We want to pick the time length of the pixels in the time–frequency map so that the signal is present in the smallest number of time–frequency pixels, as this will recover the signal with the highest likelihood. Because we do not have a model for the waveform we are searching for, we use multiple pixel lengths and run the clustering algorithm on all of them. After clusters are identified, X-Pipeline identifies which candidate clusters are likely glitches by comparing three measurements of signal energy: coherent energy consistent with GWs, coherent energy inconsistent with GWs, and sum of the signal energy in all detectors (referred to as incoherent energy). GW signals can be differentiated from noise by the ratio of coherent energy inconsistent with GWs to the incoherent energy (see Sections 2.6 and 3.4 of Sutton et al. 2010 for full details).

The primary target of this search are GWs produced from the excitation of the magnetar’s fundamental mode, which are primarily dampened by the emission of GWs (Detweiler 1975; Andersson & Kokkotas 1998). We have chosen parameters for X-Pipeline to search for signals a few hundred milliseconds long. The search window begins 4 s before the γ -rays arrive and ends 4 s after. The frequency range for the short-duration search is 64–4000 Hz, and the pixel lengths are every factor of 2 between 2 s and 1/128 s, inclusive.

3.3. STAMP

STAMP is an unmodeled, coherent, directed excess power search suitable for longer duration signals, described in more detail in Thrane et al. (2011). In short, the pipeline calculates the cross-power between the two detectors, accounting for the time delay due to the light-travel time between detectors. It then makes this into a time–frequency S/N map, where the pixel S/N is estimated from the variable $\langle \hat{Y}(t; f, \hat{\Omega},) \rangle = \text{Re}[\hat{Q}_{IJ}(t; f, \hat{\Omega})(2 \tilde{s}_I^*(t; f) \tilde{s}_J(t; f))]$.

Table 2
Upper Limits on Isotropic Energy from the Short-duration Search for the February 25 Burst from SGR 1806–20

Injection Type	Frequency (Hz)	Duration/ τ (ms)	h_{rss}	Energy (erg)
Chirplet	100	10	5.42×10^{-23}	8.49×10^{43}
Chirplet	150	6.667	4.93×10^{-23}	1.58×10^{44}
Chirplet	300	3.333	5.29×10^{-23}	7.27×10^{44}
Chirplet	1000	1	1.15×10^{-22}	3.82×10^{46}
Chirplet	1500	0.6667	1.69×10^{-22}	1.81×10^{47}
Chirplet	2000	0.5	2.32×10^{-22}	5.92×10^{47}
Chirplet	2500	0.4	3.06×10^{-22}	1.56×10^{48}
Chirplet	3000	0.3333	3.96×10^{-22}	3.65×10^{48}
Chirplet	3500	0.2857	5.30×10^{-22}	8.51×10^{48}
White noise burst	100–200	11	5.57×10^{-23}	2.09×10^{44}
White noise burst	100–200	100	7.88×10^{-23}	4.15×10^{44}
White noise burst	100–1000	11	1.00×10^{-22}	1.04×10^{46}
White noise burst	100–1000	100	1.83×10^{-22}	3.55×10^{46}
Ringdown	1500	200	1.89×10^{-22}	2.25×10^{47}
Ringdown	2500	200	2.87×10^{-22}	1.37×10^{48}
Ringdown	1500	100	1.89×10^{-22}	2.25×10^{47}
Ringdown	2500	100	2.80×10^{-22}	1.30×10^{48}

Note. For white noise bursts, we give the duration of the injection, and for the other waveforms, the characteristic time. All limits are given at 50% detection efficiency, meaning that a signal with the given parameters would be detected 50% of the time.

Here, $\tilde{s}_j(t; f)$ is the Fourier-transformed data from detector I and $\hat{Q}_{IJ}(t; f, \hat{\Omega})$ is the filter function required given the locations and orientations of the pair of detectors and the sky position $\hat{\Omega}$ of the source (Thrane et al. 2011). The ideal filter function also depends on the polarization of the incoming GWs, which is unknown. Thus, the best we can do is to use the unpolarized filter function, which causes a loss of signal power (though this loss is nearly zero for optimal sky locations). This is more fully discussed in Appendix B.

To identify signals, STAMP uses seedless clustering and searches over a large number of clusters (30 million in this search; see Section 3 of Thrane & Coughlin 2013). For clusters, we use Bézier curves, which are parameterized by three points (Thrane & Coughlin 2013).

GWs radiated through the mechanisms related to QPOs would be monochromatic, or close to it. So, it makes sense to only search for such signals. Through STAMP, this is easily accomplished by restricting the search to clusters whose frequencies change by only a small amount. This reduces the number of possible clusters, which means we get all of the benefits of searching more clusters without the additional computational cost. Restricting the frequency change too much may cause signals to be missed completely. Compromising between these, we restrict the searched clusters to those with a frequency change less than 10%.

To estimate the background for this search, we use approximately 15 hr of data from each detector collected around the time of each burst, excluding the data, coincident with the burst, that were searched for GWs (the on-source). We can then perform background experiments free of any possible

Table 3
Upper Limits on GW Strain and Energy from the Intermediate-duration Search for the February 25 Burst from SGR 1806–20

Frequency (Hz)	Tau (s)	h_{rss}		Energy (erg)	
		Half Sine-Gaussian	Ringdown	Half Sine-Gaussian	Ringdown
55	400	2.29×10^{-22}	2.43×10^{-22}	1.82×10^{44}	2.06×10^{44}
55	150	1.97×10^{-22}	2.11×10^{-22}	1.35×10^{44}	1.55×10^{44}
150	400	1.32×10^{-22}	1.37×10^{-22}	4.52×10^{44}	4.86×10^{44}
150	150	1.14×10^{-22}	1.22×10^{-22}	3.37×10^{44}	3.89×10^{44}
450	400	1.69×10^{-22}	1.79×10^{-22}	6.62×10^{45}	7.47×10^{45}
450	150	1.78×10^{-22}	1.83×10^{-22}	7.43×10^{45}	7.83×10^{45}
750	400	2.56×10^{-22}	2.70×10^{-22}	4.21×10^{46}	4.69×10^{46}
750	150	2.11×10^{-22}	2.37×10^{-22}	2.87×10^{46}	3.61×10^{46}
1550	400	5.86×10^{-22}	6.22×10^{-22}	9.21×10^{47}	1.03×10^{48}
1550	150	4.38×10^{-22}	4.58×10^{-22}	5.16×10^{47}	5.62×10^{47}

Note. All limits are at 50% detection efficiency.

coincident GW signal by pairing data taken at different times as if they were coincident. Then, breaking up the background data into 33 segments, we generate 1056 background experiments. Each of these is run in exactly the same way as the on-source analysis, giving an estimate of the S/N that can be expected from detector noise. The resulting distributions for the background data for each burst, along with the on-source results, are shown in Figure 2.

With unlimited computing power, we would calculate upper limits by adding software injections of increasing amplitude until the desired fraction of injections are recovered. However, this is prohibitively expensive in computing time. Instead, at each amplitude for the injection, we search only over a few previously identified clusters. To pick those clusters, we do a full run using the seedless algorithm with 15 injections at varied amplitudes around the expected recovery threshold and identify clusters that recover the injection, setting the same random seed as was used for the on-source recovery. We then analyze a large number of injections using only the pre-identified clusters and calculate the maximum S/N of those clusters. The injections at all amplitudes are done with the same time–frequency parameters. This allows us to efficiently recover the injection by searching a small fraction of the total clusters. This is shown to work as expected in Appendix A.

Because choosing a random seed also chooses which clusters will be searched, this value can affect the final upper limit values. This effect is limited by using a large number of clusters (30 million), and analysis performed with different seeds shows this effect leads to about a 10% uncertainty in the resulting upper limit value. However, this is not a completely new source of error—changing the seed is functionally equivalent to changing the time–frequency location of the software injections. In addition, the on-source analysis uses only one seed because it is only run once, so this uncertainty is a manifestation of the random nature of the search.

4. Results and Discussion

No signals were found by either the short- or intermediate-duration searches. We present the results and upper limits on GW strain and energy for each analysis below.

4.1. Short-duration Search Upper Limits

No significant signal was found by X-Pipeline. After glitch rejection, the most significant cluster for the February 25 burst had a p -value of 0.63.

Following the previous f-mode search (Abadie et al. 2012), we injected white noise bursts (frequencies: 100–200 Hz and 100–1000 Hz; durations: 11 and 100 ms), ringdowns (damped sinusoids, at frequencies: 1500 and 2500 Hz; time constants: 100 and 200 ms), and chirplets (chirping sine-Gaussians; this differs from the prior search, which used sine-Gaussians). The best limits for the white noise bursts were for the 11 ms long bursts in the 100–200 Hz band, at 2.1×10^{44} erg in total isotropic energy and h_{rss} of 5.6×10^{-23} at the detectors. We are most sensitive to ringdowns at 1500 Hz and a time constant of 100 ms, with an upper limit of 2.3×10^{47} erg and h_{rss} of 1.9×10^{-22} . Directly comparing the h_{rss} limits to Abadie et al. (2011), we see that limits have improved by roughly a factor of 10, though the ringdowns we used had slightly different parameters. Comparing to Abadie et al. (2012), which provided only energy upper limits assuming a distance of 3.6 Mpc, we see an improvement of a factor of 60 after correcting for the larger distance. This corresponds to roughly a factor of 8 improvement in h_{rss} limits. A full list of upper limits for the waveforms tested is found in Table 2.

4.2. Intermediate-duration Search Upper Limits

To calculate upper limits, we add software injections of two waveforms (half sine-Gaussians and exponentially decaying sinusoids) at five frequencies (55, 150, 450, 750, and 1550 Hz) and at two timescales (150 and 400 s). Reported upper limits are for 50% recovery efficiency, where recovery is defined as finding a cluster, at the same time and frequency as the injection, with S/N greater than that of the on-source (for the February 25 event, it was 6.09). Full results are shown in Table 3.

Due to the improved sensitivity of advanced LIGO, we are able to set strain upper limits about a factor of 10 lower than the previous search during initial LIGO (Quitzow-James et al. 2017); see Figure 3. Unlike the previous search, this search showed little difference in h_{rss} sensitivity between the two injection lengths. STAMP has been refined to improve power spectral density estimation, which explains the small gap between the injection timescales for this search.

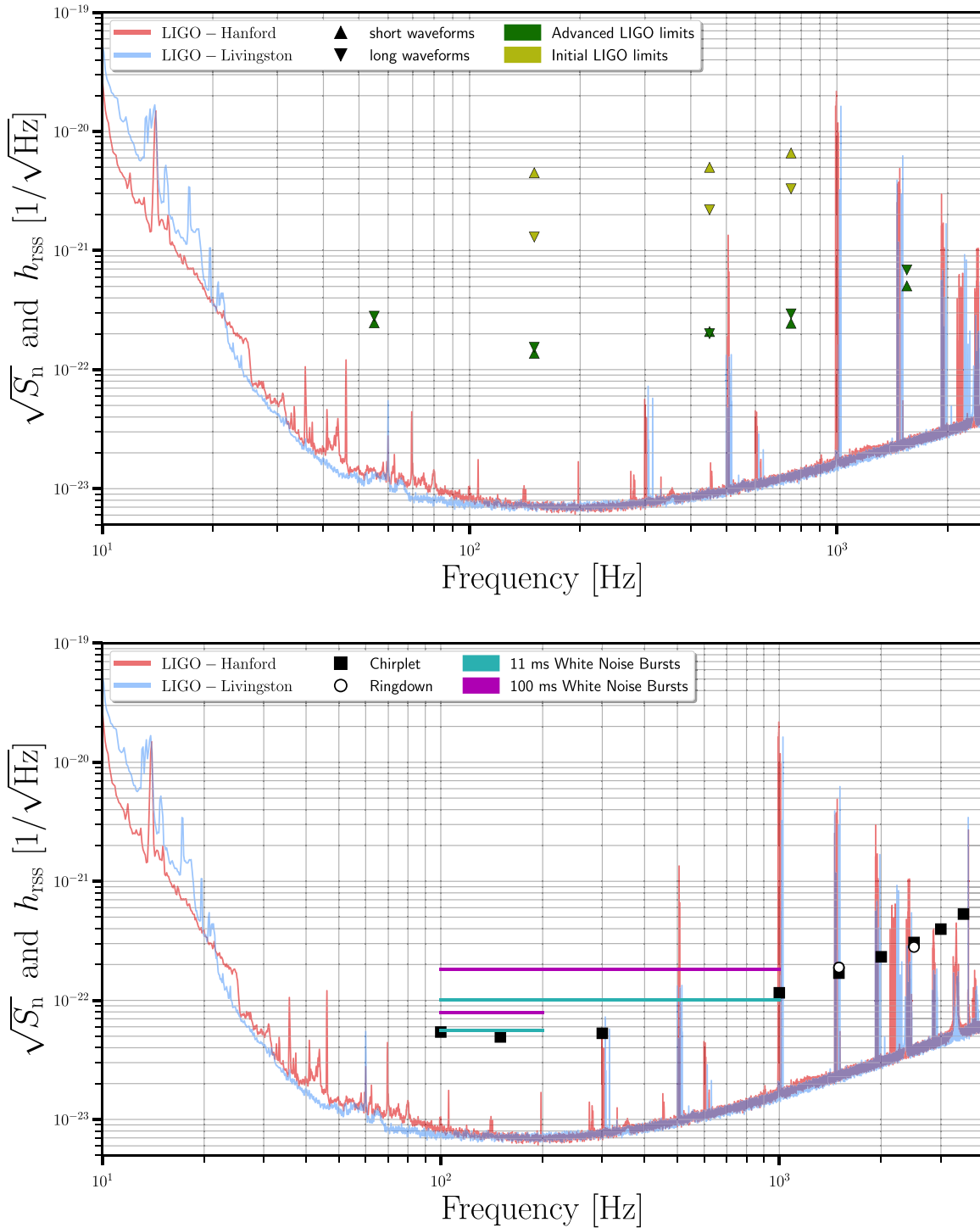


Figure 3. Upper limits for the the intermediate-duration search (above) and short-duration search (below), along with the sensitivity of the detectors. We plot h_{rss} at 90% detection efficiency for the intermediate-duration search here to allow direct comparison to published figures for the previous search in initial LIGO (Quitow-James et al. 2017). Short-duration limits are for 50% efficiency as before. The advanced-duration limits are for the February 25 burst from SGR 1806–20 during the second observing run, and detector sensitivity is calculated from data during the analysis window. The data used to create this figure are available.

4.3. Discussion

This search has set the strongest upper limits on the short- and intermediate-duration GW emission associated with magnetar bursts. The energy limits, which are as low as 10^{44} – 10^{47} erg, are now well below the EM energy scale of magnetar giant flares (10^{46} erg). The short bursts analyzed here

were much weaker than a giant flare (see Table 1), so for these bursts, the limit is much larger than the observed electromagnetic energy. In addition, these limits assume ideal orientation of the magnetar (both sky position and polarization of produced GWs). The impact of other polarizations on the intermediate-duration search is discussed in Appendix B and plotted in Figure 4.

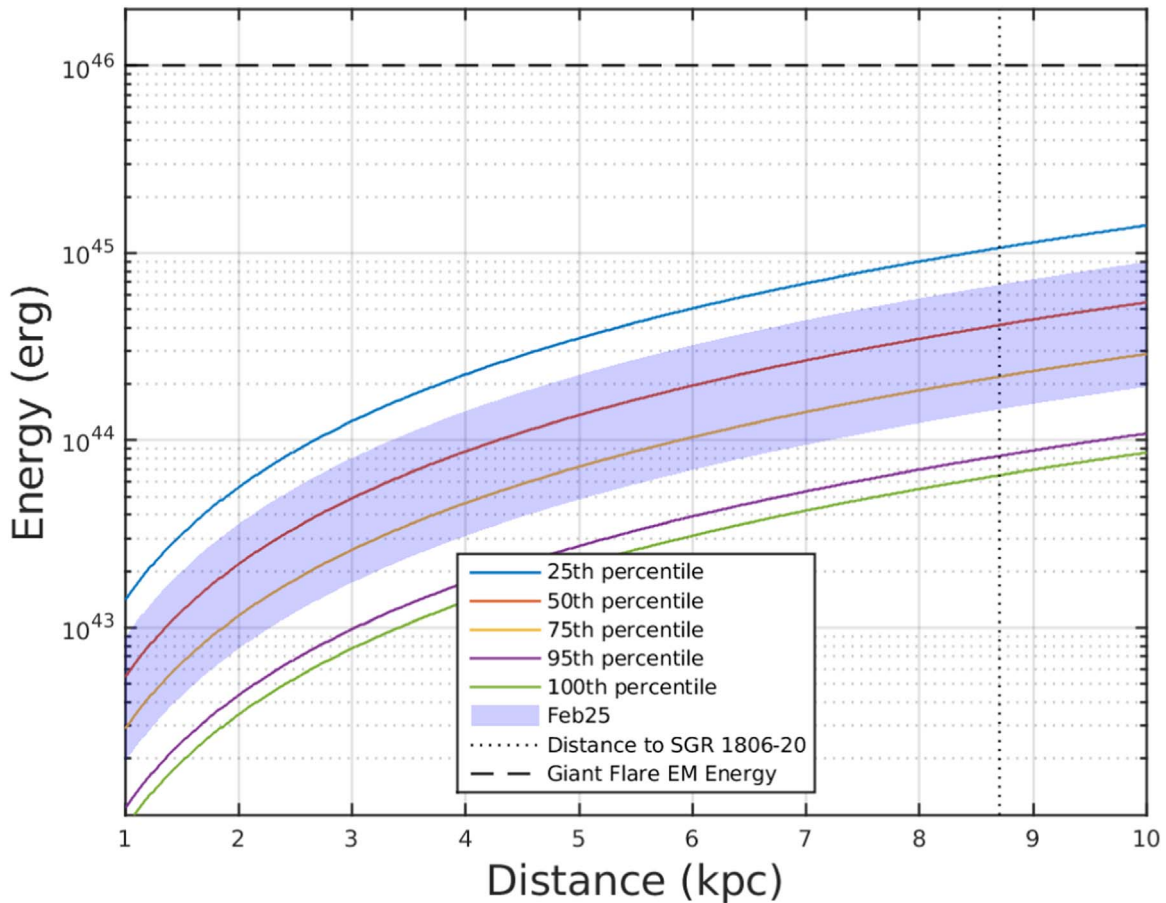


Figure 4. Minimum detectable energy for the intermediate-duration search vs. distance for SGR 1806–20 for varied sky locations and GW polarizations at 55 Hz. The lines show how the variation in sky position (caused by Earth’s rotation) and polarization (assumed to be random) affects the sensitivity; the purple 95th percentile line indicates that the network sensitivity will be better than indicated by that line only 5% of the time. The shaded region indicates the sensitivity to GW energy from the burst on February 25. Here, the uncertainty is only due to the unknown polarization. The data used to create this figure are available.

The upper limits set by this search are still far above the GW energy from f-mode excitation during a giant flare according to Zink et al. (2012), unless the magnetic field strength is far higher than the currently accepted value of 2×10^{15} G (Olausen & Kaspi 2014). Using Equation (2) from Zink et al. (2012), f-mode GW emission from a giant flare would be about 1.4×10^{38} erg. A surface magnetic field of 1.8×10^{16} G would be required to reach the best upper limit found with the short-duration source.

As the LIGO detectors increase in sensitivity, these upper limits will improve and will be well positioned to place meaningful limits on emitted GW energy in the event of a future nearby magnetar giant flare.

The authors gratefully acknowledge the support of the United States National Science Foundation (NSF) for the construction and operation of the LIGO Laboratory and Advanced LIGO as well as the Science and Technology Facilities Council (STFC) of the United Kingdom, the Max-Planck-Society (MPS), and the State of Niedersachsen/Germany for support of the construction of Advanced LIGO and construction and operation of the GEO600 detector. Additional support for Advanced LIGO was provided by the Australian Research Council. The authors gratefully acknowledge the Italian Istituto Nazionale di Fisica Nucleare (INFN),

the French Centre National de la Recherche Scientifique (CNRS), and the Foundation for Fundamental Research on Matter supported by the Netherlands Organisation for Scientific Research for the construction and operation of the Virgo detector and the creation and support of the EGO consortium. The authors also gratefully acknowledge research support from these agencies as well as by the Council of Scientific and Industrial Research of India, the Department of Science and Technology, India, the Science & Engineering Research Board (SERB), India, the Ministry of Human Resource Development, India, the Spanish Agencia Estatal de Investigación, the Vicepresidència i Conselleria d’Innovació Recerca i Turisme and the Conselleria d’Educació i Universitat del Govern de les Illes Balears, the Conselleria d’Educació Investigació Cultura i Esport de la Generalitat Valenciana, the National Science Centre of Poland, the Swiss National Science Foundation (SNSF), the Russian Foundation for Basic Research, the Russian Science Foundation, the European Commission, the European Regional Development Funds (ERDF), the Royal Society, the Scottish Funding Council, the Scottish Universities Physics Alliance, the Hungarian Scientific Research Fund (OTKA), the Lyon Institute of Origins (LIO), the Paris Île-de-France Region, the National Research, Development and Innovation Office Hungary (NKFIH), the National Research Foundation of Korea, Industry Canada and the Province of

Ontario through the Ministry of Economic Development and Innovation, the Natural Science and Engineering Research Council Canada, the Canadian Institute for Advanced Research, the Brazilian Ministry of Science, Technology, Innovations, and Communications, the International Center for Theoretical Physics South American Institute for Fundamental Research (ICTP-SAIFR), the Research Grants Council of Hong Kong, the National Natural Science Foundation of China (NSFC), the Leverhulme Trust, the Research Corporation, the Ministry of Science and Technology (MOST), Taiwan, and the Kavli Foundation. The authors gratefully acknowledge the support of the NSF, STFC, MPS, INFN, CNRS, and the State of Niedersachsen/Germany for provision of computational resources.

Appendix A Validation of the Injection Recovery Method

In Section 3, we described the way we obtain the precise detectability threshold of injected waveforms. Given that this method is an approximation of the full search protocol, we check to see how closely the results match that of the full search. Figure 5 shows the result of this test, run over 100 injection trials. A point falling below the diagonal indicates that the noise and injected signal conspire together in such a way that the cluster with the highest S/N is one that had not been previously identified. This test indicates that this happens infrequently. On average, we recover 98% of the S/N that is found by the full search.

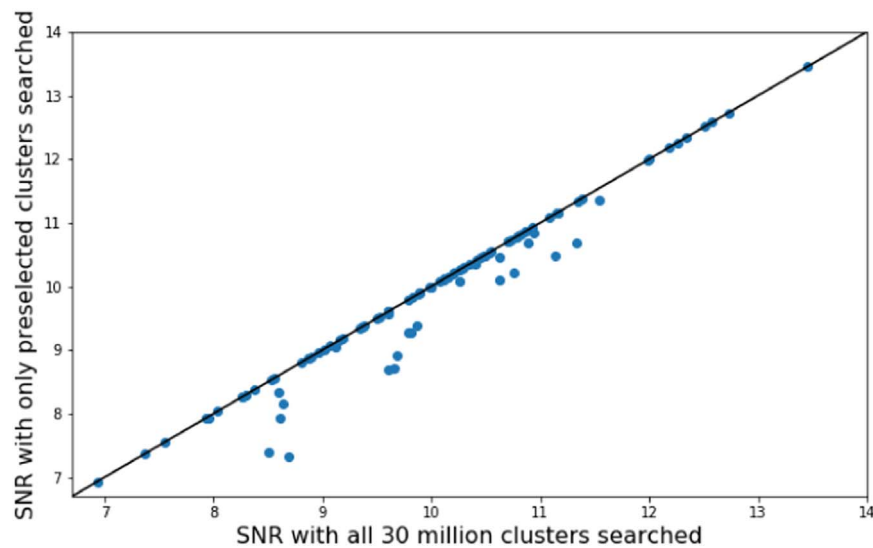


Figure 5. Direct comparison of the S/N recovered by a full run of 30 million clusters and a run with only a few previously selected clusters. This shows that this method is highly effective in recovering the injected signal, at a small fraction of the computational cost.

Appendix B STAMP Polarization

The cross-power of a pixel in the time–frequency map is calculated with $\hat{Y} \equiv \text{Re} [\tilde{Q}_{IJ}(t; f, \hat{\Omega}) C_{IJ}(t; f)]$, where $\tilde{Q}_{IJ}(t; f, \hat{\Omega})$ is the filter function that depends on the polarization of the GWs. Because we do not know the polarization of the GWs that we are looking for, we use an approximation of the ideal filter function. We choose the unpolarized filter function $\tilde{Q}_{IJ}(t; f, \hat{\Omega}) = \frac{1}{\epsilon_{IJ}(t; \hat{\Omega})} e^{2\pi i f \hat{\Omega} \cdot \Delta \vec{x}_{IJ} / c}$ (Thrane et al. 2011). The second term in this equation corrects for a difference in phase due to different travel distances from the source to the two detectors. For this discussion, we will set it to 1 for simplicity.

If the GWs emitted from magnetars are due to a pure quadrupole, we expect them to be polarized elliptically according to standard linearized gravity, with the polarization depending on the orientation of the source’s time-changing quadrupole moment with respect to our detectors.

Using Equation A48 from Thrane et al. (2011), we can see how the cross-power of an individual pixel will change with changing polarization. In Figure 6, we plot this parametrically

in the complex plane for two of the bursts analyzed. The main effect of the filter function is to pick a phase (the cross-power is multiplied by the filter function, then the real part is taken). The unpolarized filter function sets that phase to zero, so the imaginary part of the cross-power is ignored, which limits the sensitivity to nearly all elliptically polarized waveforms. Because the time–frequency map is normalized by the average value of the power spectral density nearby in time, the magnitude of the filter function only matters if it changes over the course of a time–frequency map.

In addition, for some polarizations, the cross-power is negative, which will result in pixels in the S/N map being negative. For this reason, these signals, no matter how large in amplitude, would be missed by this search. However, these signals produce little cross-power (as evidenced by how close they are to zero) such that the likelihood of detecting them even with the ideal filter function is low. It is possible to recover these by taking the absolute value of each cluster, but doing this is roughly equivalent to running the search twice with opposite phase filter functions. Thus, it will double the background.

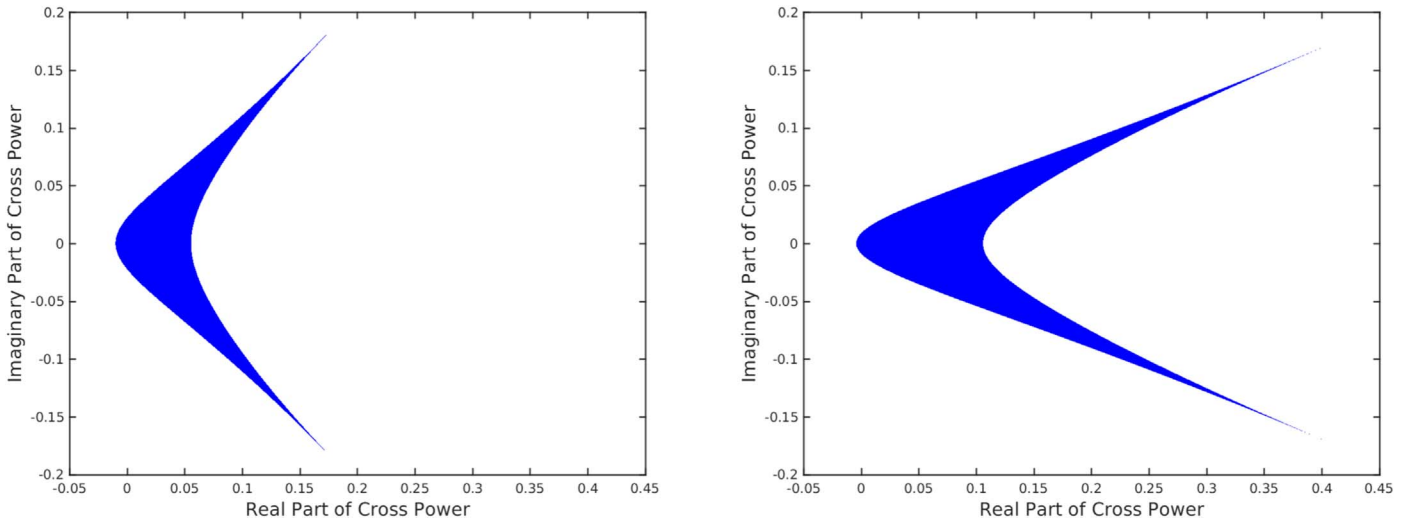


Figure 6. Parametric plots of the complex-valued cross-power, due to elliptically polarized signals of varying polarizations from two different sky locations (left: SGR 1806–20 during the event on April 29; right: SGR 1806–20 during the event on February 25). The polarization of incoming GWs is defined by two angles, ι and ψ . ι is the angle between the vector from Earth to the source and the source’s rotation vector, while ψ indicates the orientation of the source’s rotation vector when projected onto a plane perpendicular to the propagation vector. The ends of the boomerang are at $\iota = 0, \pi$; changing ψ changes the real part only. For ideal sky positions, the boomerang collapses to the real axis and reaches about 0.95. It does not reach 1 because the detectors are not aligned.

Appendix C Supplementary Data

Figure 7 shows *Swift* BAT's data for the February 25 and April 29 bursts from SGR 1806–20.

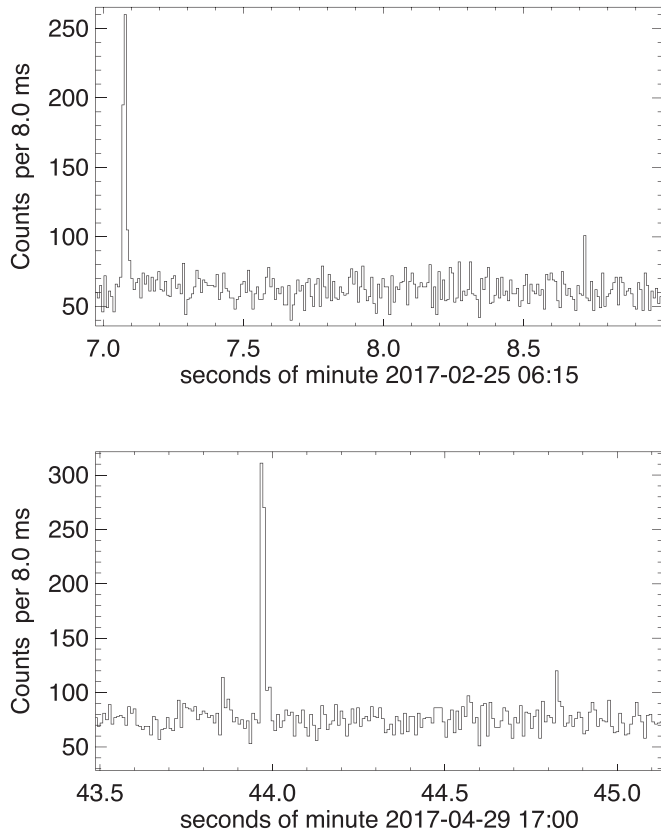


Figure 7. *Swift* BAT's data for the February 25 and April 29 bursts from SGR 1806–20. Images courtesy of David M. Palmer.

References

- Aasi, J., Abbott, B. P., Abbott, R., et al. 2015, *CQGra*, 32, 074001
- Abadie, J., Abbott, B. P., Abbott, R., et al. 2011, *ApJL*, 734, L35
- Abadie, J., Abbott, B. P., Abbott, T. D., et al. 2012, *ApJ*, 755, 2
- Abbott, B., Abbott, R., Adhikari, R., et al. 2007, *PhRvD*, 76, 062003
- Abbott, B. P., Abbott, R., Abbott, T. D., et al. 2016a, *PhRvL*, 116, 241103
- Abbott, B. P., Abbott, R., Abbott, T. D., et al. 2016b, *PhRvL*, 116, 061102
- Abbott, B. P., Abbott, R., Abbott, T. D., et al. 2017a, *ApJ*, 841, 89
- Abbott, B. P., Abbott, R., Abbott, T. D., et al. 2017b, *PhRvL*, 118, 221101
- Abbott, B. P., Abbott, R., Abbott, T. D., et al. 2017c, *ApJL*, 851, L35
- Abbott, B. P., Abbott, R., Abbott, T. D., et al. 2017d, *PhRvL*, 119, 141101
- Abbott, B. P., Abbott, R., Abbott, T. D., et al. 2017e, *PhRvL*, 119, 161101
- Abbott, B. P., Abbott, R., Adhikari, R., et al. 2008, *PhRvL*, 101, 211102
- Abbott, B. P., Abbott, R., Adhikari, R., et al. 2009, *ApJL*, 701, L68
- Acernese, F., Agathos, M., Agatsuma, K., et al. 2015, *CQGra*, 32, 024001
- Andersson, N., & Kokkotas, K. D. 1998, *MNRAS*, 299, 1059
- Atwood, W. B., Abdo, A. A., Ackermann, M., et al. 2009, *ApJ*, 697, 1071
- Braithwaite, J., & Spruit, H. 2006, *A&A*, 450, 1097
- Corsi, A., & Owen, B. J. 2011, *PhRvD*, 83, 104014
- Detweiler, S. L. 1975, *ApJ*, 197, 203
- Gehrels, N., Chincarini, G., Giommi, P., et al. 2004, *ApJ*, 611, 1005
- Huppenkothen, D., Heil, L. M., Watts, A. L., & Göğüş, E. 2014a, *ApJ*, 795, 114
- Huppenkothen, D., D'Angelo, C., Watts, A. L., et al. 2014b, *ApJ*, 787, 128
- Ioka, K. 2001, *MNRAS*, 327, 639
- Israel, G. L., Belloni, T., Stella, L., et al. 2005, *ApJL*, 628, L53
- Kalmus, P., Cannon, K. C., Márka, S., & Owen, B. J. 2009, *PhRvD*, 80, 042001
- Kalmus, P., Khan, R., Matone, L., & Márka, S. 2007, *CQGra*, 24, S659
- Levin, Y., & van Hoven, M. 2011, *MNRAS*, 418, 659
- Matone, L., & Márka, S. 2007, *CQGra*, 24, S649
- Mereghetti, S., Pons, J. A., & Melatos, A. 2015, *SSRv*, 191, 315
- Olausen, S. A., & Kaspi, V. M. 2014, *ApJS*, 212, 6
- Quitow-James, R. 2016, PhD thesis, Univ. Oregon
- Quitow-James, R., Brau, J., Clark, J. A., et al. 2017, *CQGra*, 34, 164002
- Sathyaprakash, B. S., & Schutz, B. F. 2009, *LRR*, 12, 2
- Strohmayer, T. E., & Watts, A. L. 2005, *ApJL*, 632, L111
- Sutton, P. J., Jones, G., Chatterji, S., et al. 2010, *NJPh*, 12, 053034
- Thompson, C., & Duncan, R. C. 1995, *MNRAS*, 275, 255
- Thrane, E., & Coughlin, M. 2013, *PhRvD*, 88, 083010
- Thrane, E., & Coughlin, M. 2014, *PhRvD*, 89, 063012
- Thrane, E., Kandhasamy, S., Ott, C. D., et al. 2011, *PhRvD*, 83, 083004
- Woods, P. M., & Thompson, C. 2006, *Soft Gamma Repeaters and Anomalous X-ray Pulsars: Magnetar Candidates* (Cambridge: Cambridge Univ. Press), 547
- Zink, B., Lasky, P. D., & Kokkotas, K. D. 2012, *PhRvD*, 85, 024030